STANFORD
AERONAUTICS &
ASTRONAUTICS

Applications:

A new boundary layer integral method,

Rough wall pipe flow

Brian Cantwell
Stanford University
May 14, 2025

Zero angle of attack viscous drag of Joukowsky and NACA 0012 airfoils

Choose the airfoil nose radius, r, as the characteristic length scale. Let $\xi = x/r$ where x is the coordinate along the airfoil surface.

Assume the UVP holds beginning at the forward stagnation point. That assumes that the laminar-turbulent transition Reynolds number is close to the minimum required to sustain turbulent flow, $R_{\tau\ \text{transition}} \approx 200$. In other words, the UVP corresponds to a fully tripped boundary layer. Later comparisons are with tripped airfoil data.

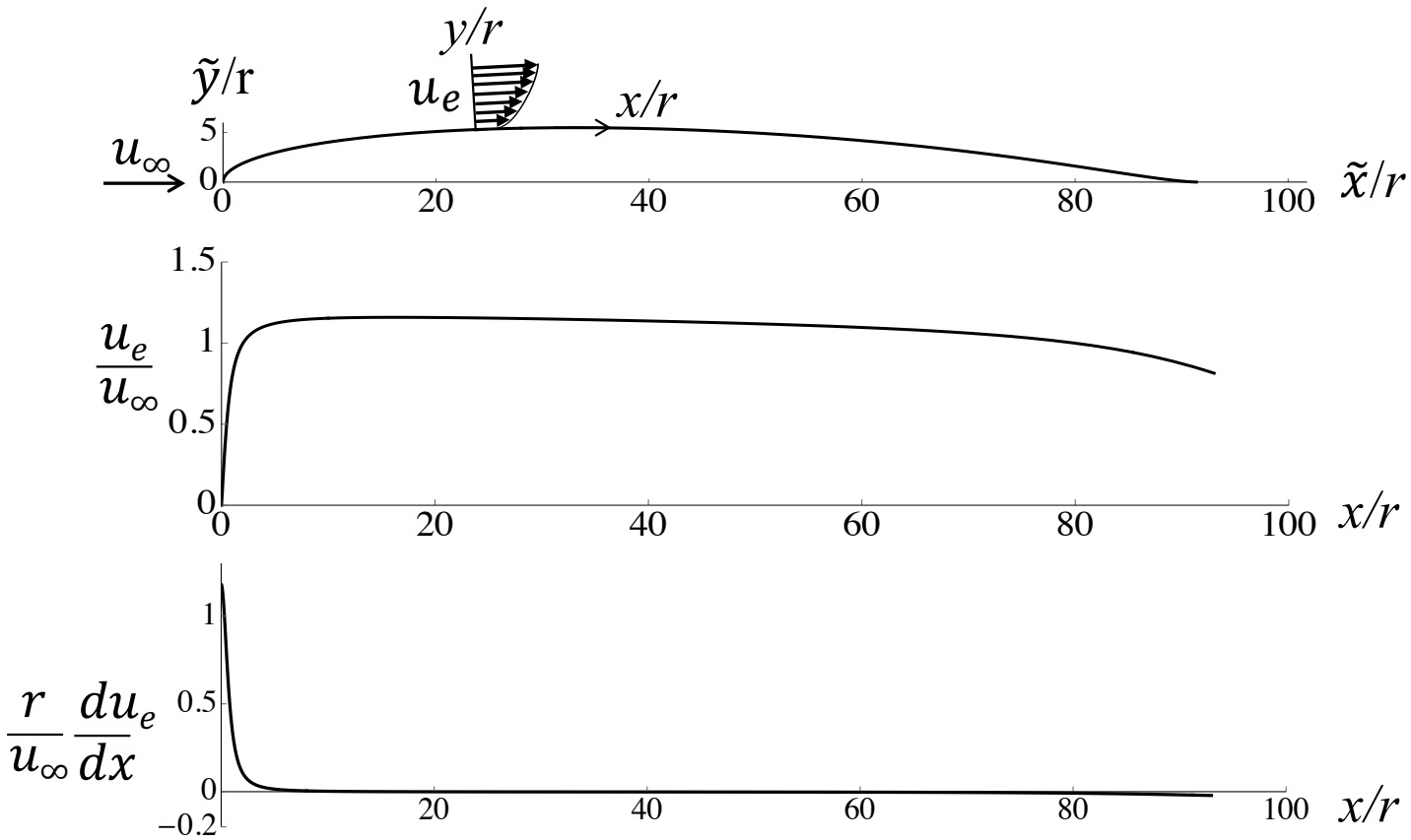

Reynolds number based on nose radius

$$R_e = \frac{u_\infty r}{\nu}$$

From potential flow

$$\frac{u_e}{u_\infty} = U(\xi)$$

$$\xi = \frac{x}{r}$$

We use the UVP beginning at the forward stagnation point. How accurate is this assumption?

Use the Hiemenz solution to approximate the stagnation point flow near the leading edge

Reynolds number based on nose radius

$$R_e = \frac{u_\infty r}{\nu}$$

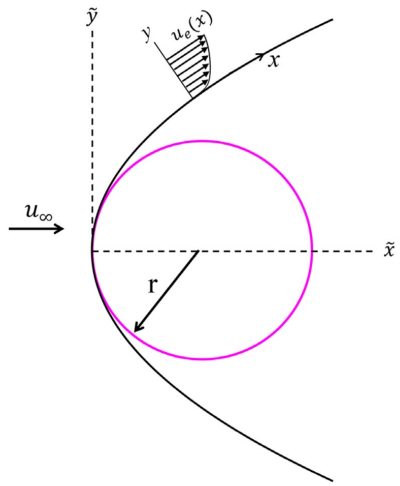

FIG. 2. Coordinate notation near the wing leading edge.

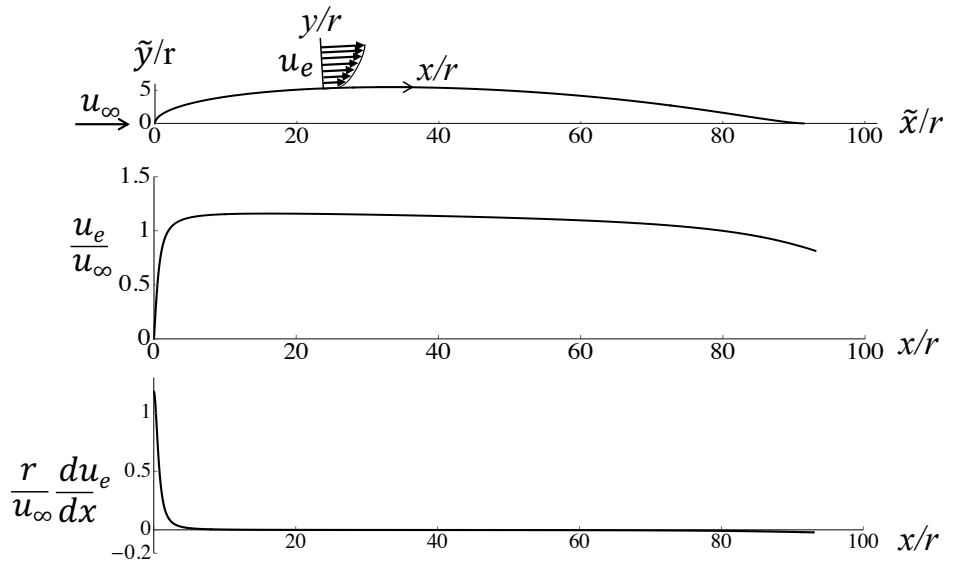

To model the leading edge flow we will use the inviscid solution about an elliptic wing presented by Van Dyke. Let

$$\alpha \equiv 1 + \left(2\frac{r}{c}\right)^{1/2}$$

The coordinate of the upper surface of an ellipse with the leading edge located at $\tilde{x}$ /c = 0 is

$$\frac{\tilde{y}}{c} = \frac{1}{2}(\alpha - 1)\left(1 - \left(2\frac{\tilde{x}}{c} - 1\right)^2\right)^{1/2}$$

The surface velocity is

$$U\left(\frac{\tilde{x}}{c}\right)=\frac{\alpha}{\left(1+(\alpha-1)^2\dfrac{\left(2\dfrac{\tilde{x}}{c}-1\right)^2}{1-\left(2\dfrac{\tilde{x}}{c}-1\right)^2}\right)^{1/2}}$$

The coordinate $x(\tilde{x})$ along the wing surface is

$$\frac{x}{c}=\frac{1}{2}\left(E\left(\frac{\pi}{2},1-\alpha\right)-E\left(\text{Arcsin}\left(1-2\frac{\tilde{x}}{c}\right),1-\alpha\right)\right)$$

where the function $E(\theta,1-\alpha)$ is the incomplete elliptic integral of the second kind. The following limits are found to hold near the leading edge. Recall $\xi=x/r$.

$$\lim_{\frac{\tilde{x}}{c}\to 0}\frac{\tilde{y}}{c}=\frac{x}{c},$$

$$\lim_{\frac{\tilde{x}}{c}\to 0}\frac{x}{c}=(\alpha-1)\left(\frac{\tilde{x}}{c}\right)^{1/2},$$

$$\lim_{\frac{\tilde{x}}{c}\to 0}U=\frac{2\alpha}{\alpha-1}\left(\frac{\tilde{x}}{c}\right)^{1/2},$$

$$\lim_{\frac{\tilde{x}}{c}\to 0}U=\frac{2\alpha}{(\alpha-1)^2}\left(\frac{x}{c}\right),$$

$$\lim_{\frac{\tilde{x}}{c}\to 0}U=\alpha\ \xi.$$

STANFORD
AERONAUTICS &
ASTRONAUTICS

The Hiemenz solution near the leading edge

$$\eta = \alpha^{1/2}\left(\frac{u_\infty r}{\nu}\right)^{1/2}\left(\frac{y}{r}\right)$$

$$\frac{v(x,y)}{u_\infty} = -\alpha^{1/2}\left(\frac{\nu}{u_\infty r}\right)f(\eta)$$

$$\frac{u(x,y)}{u_\infty} = \alpha\xi f'(\eta)$$

$$\frac{\Omega(x,y)r}{u_\infty} = -\frac{r}{u_\infty}\frac{\partial u}{\partial y} = -\alpha^{3/2}\left(\frac{u_\infty r}{\nu}\right)^{1/2}\xi f''(\eta)$$

Substitute into the vorticity equation.

$$u\frac{\partial \Omega}{\partial x} + v\frac{\partial \Omega}{\partial y} - \nu\frac{\partial^2 \Omega}{\partial x^2} - \nu\frac{\partial^2 \Omega}{\partial y^2} = 0$$

The result is

$$\alpha^{1/2}(\nu r u_\infty)^{1/2}\left(f''''(\eta) + f(\eta)f'''\prime(\eta) - f'(\eta)f''(\eta)\right) = 0$$

This fourth-order ordinary differential equation can be integrated once leading to the third-order equation governing the Hiemenz solution.

$$f'''(\eta) + f(\eta) f''(\eta) + 1 - f'(\eta)^2 = 0$$
$$f(0) = 0, \quad f'(0) = 0, \quad f'(\infty) = 1$$

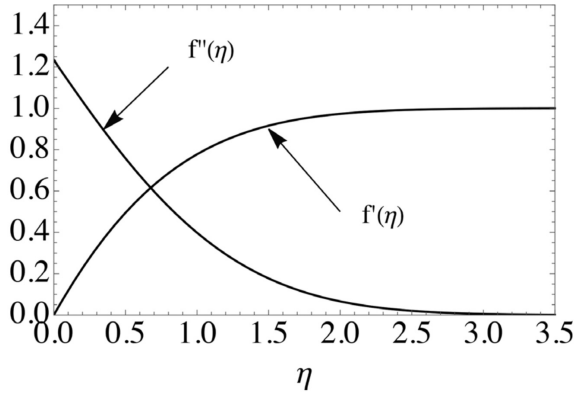

FIG. 20. Hiemenz streamwise velocity and vorticity.

Near the leading edge, the Hiemenz solution leads to the following limits:

$$\lim_{\xi \to 0} \left(\frac{u_\tau}{u_e} \right)^2 = \frac{f''(0)}{\alpha^{1/2} R_e{}^{1/2}\ \xi},$$
$$\lim_{\xi \to 0} \frac{\delta_1 u_\infty}{\nu} = \frac{c_1}{\alpha^{1/2} R_e{}^{1/2}},$$
$$\lim_{\xi \to 0} \frac{\delta_2 u_\infty}{\nu} = \frac{c_2}{\alpha^{1/2} R_e{}^{1/2}},$$
$$\lim_{\xi \to 0} R_\tau = \eta_h f''(0)^{1/2} \alpha^{1/4} R_e{}^{1/4}\ \xi^{1/2},$$

The shape factor of the Hiemenz flow at the forward stagnation point is $H = \frac{\delta_1}{\delta_2} = 2.216$, which can be compared to $H = 2.5$ for channel flow and $H = 2.604$ for the ZPG Blasius boundary layer.

where $f''(0) = 1.232\,59$, $c_1 = 0.647\,836$, and $c_2 = 0.292\,282$

Recall the following functions

The boundary layer friction law

$$\frac{u_e}{u_\tau} = \int_0^{R_\tau} \frac{2\left(1 - \frac{s}{R_\tau}\right)}{1 + \left(1 + 4\lambda^2\left(1 - \frac{s}{R_\tau}\right)\right)^{1/2}} ds \equiv F_0$$

Displacement thickness Reynolds number in wall units

$$R_{\delta_1} = \frac{u_e \delta_1}{\nu} = \frac{u_e}{u_\tau} \int_0^{R_\tau} \left(1 - \frac{u_\tau}{u_e} u^+\right) dy^+ \equiv F_1$$

Momentum thickness Reynolds number in wall units

$$R_{\delta_2} = \frac{u_e \delta_2}{\nu} = \int_0^{R_\tau} u^+ \left(1 - \frac{u_\tau}{u_e} u^+\right) dy^+ \equiv F_2$$

Derivative of the momentum thickness Reynolds number in wall units

$$\frac{dF_2}{dR_\tau} \equiv F_3$$

The UVP near the leading edge

In the UVP integral boundary layer method the simplest approach will be used where the UVP is assumed to apply all the way from the forward stagnation point of the airfoil. Therefore, it is important to consider the degree of error associated with this assumption by comparing it with the "exact" Hiemenz solution.

The UVP approaches the laminar channel profile at the wing leading edge. From this profile, the following limits can be determined.

$$\lim_{R_\tau \to 0} F_0 = \frac{R_\tau}{2},$$

$$\lim_{R_\tau \to 0} F_1 = \frac{{R_\tau}^2}{6},$$

$$\lim_{R_\tau \to 0} F_2 = \frac{{R_\tau}^2}{15},$$

$$\lim_{R_\tau \to 0} F_3 = \frac{2R_\tau}{15}.$$

Substitute these limits into the Karman equation. The result is

$$\frac{d}{d\xi}\left(\frac{R_\tau{}^4}{120}\right) = R_e U - \left(\frac{R_\tau{}^4}{120}\right)\frac{1}{U}\frac{dU}{d\xi}$$

with the integral

$$\lim_{R_\tau \to 0} R_\tau = \left(\frac{120 R_e}{U^7}\int_0^\xi U^8 d\xi\right)^{\frac{1}{4}}$$

where the initial condition U(0) = 0 has been used. Substitute $U = \alpha\xi$

$$\lim_{R_\tau \to 0} R_\tau = \left(\frac{40}{3}\right)^{1/4} \alpha^{1/4} R_e{}^{1/4}\ \xi^{1/2}$$

Heimenz limit

$$\lim_{\xi\to 0}\left(\frac{u_\tau}{u_e}\right)^2 = \frac{f''(0)}{\alpha^{1/2} R_e{}^{1/2}\ \xi},$$

$$\lim_{\xi\to 0}\frac{\delta_1 u_\infty}{\nu} = \frac{c_1}{\alpha^{1/2} R_e{}^{1/2}},$$

$$\lim_{\xi\to 0}\frac{\delta_2 u_\infty}{\nu} = \frac{c_2}{\alpha^{1/2} R_e{}^{1/2}},$$

$$\lim_{\xi\to 0} R_\tau = \eta_h f''(0)^{1/2}\alpha^{1/4} R_e{}^{1/4}\ \xi^{1/2},$$

Compare the UVP limit to the Hiemenz limit, let $\eta_h = 2.381$ corresponding to $u/u_e = 0.99$.

$$\lim_{R_\tau \to 0}\frac{R_{\tau UVP}}{R_{\tau Hiemenz}} = \frac{\left(\frac{40}{3}\right)^{1/4}}{2.381 f''(0)^{1/2}} = 0.723$$

The laminar limiting profile of the UVP can be expressed in terms of η by noting that $y/\delta_h = \eta/\eta_h$.

$$\frac{u(x,y)}{u_\infty} = \alpha\ \xi\left(\frac{2\eta}{\eta_h}\right)\left(1 - \frac{1}{2}\frac{\eta}{\eta_h}\right)$$

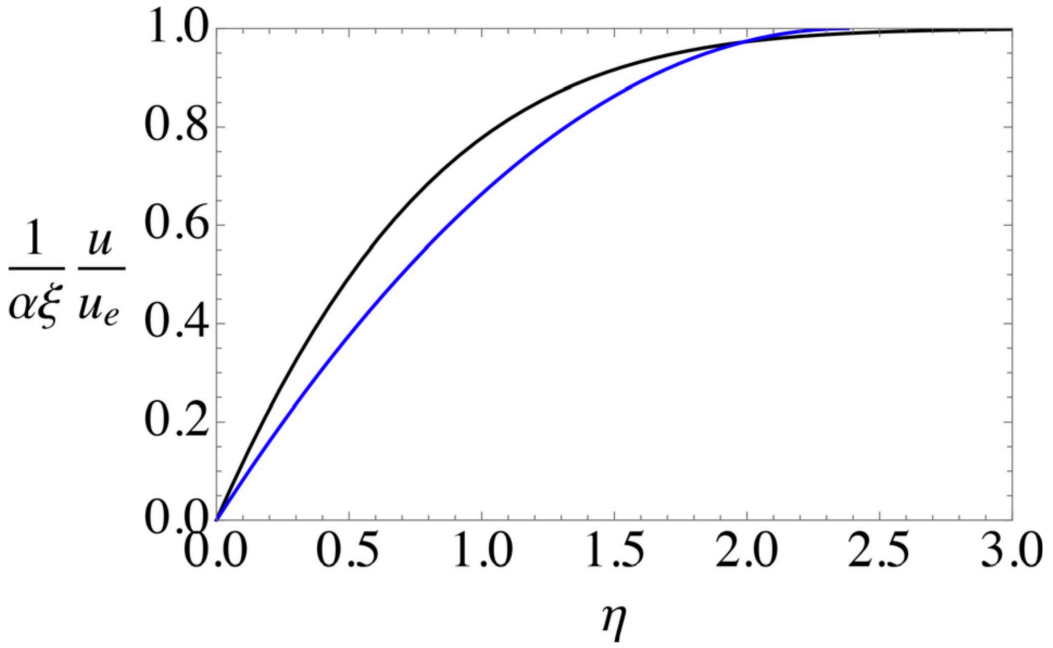

FIG. 21. Comparison between the Hiemenz velocity profile (black) and UVP (blue) near the forward stagnation point.

The conclusion from this discussion is that near the leading edge, the UVP limit has the same dependence on α, Re, and ξ as the "exact" Hiemenz limit but the magnitude of R_τ, and therefore, the friction is about 28% below the Hiemenz limit. Keeping this in mind, the UVP will be assumed to apply beginning at the leading edge in the airfoil in the examples discussed in later slides.

The UVP friction law

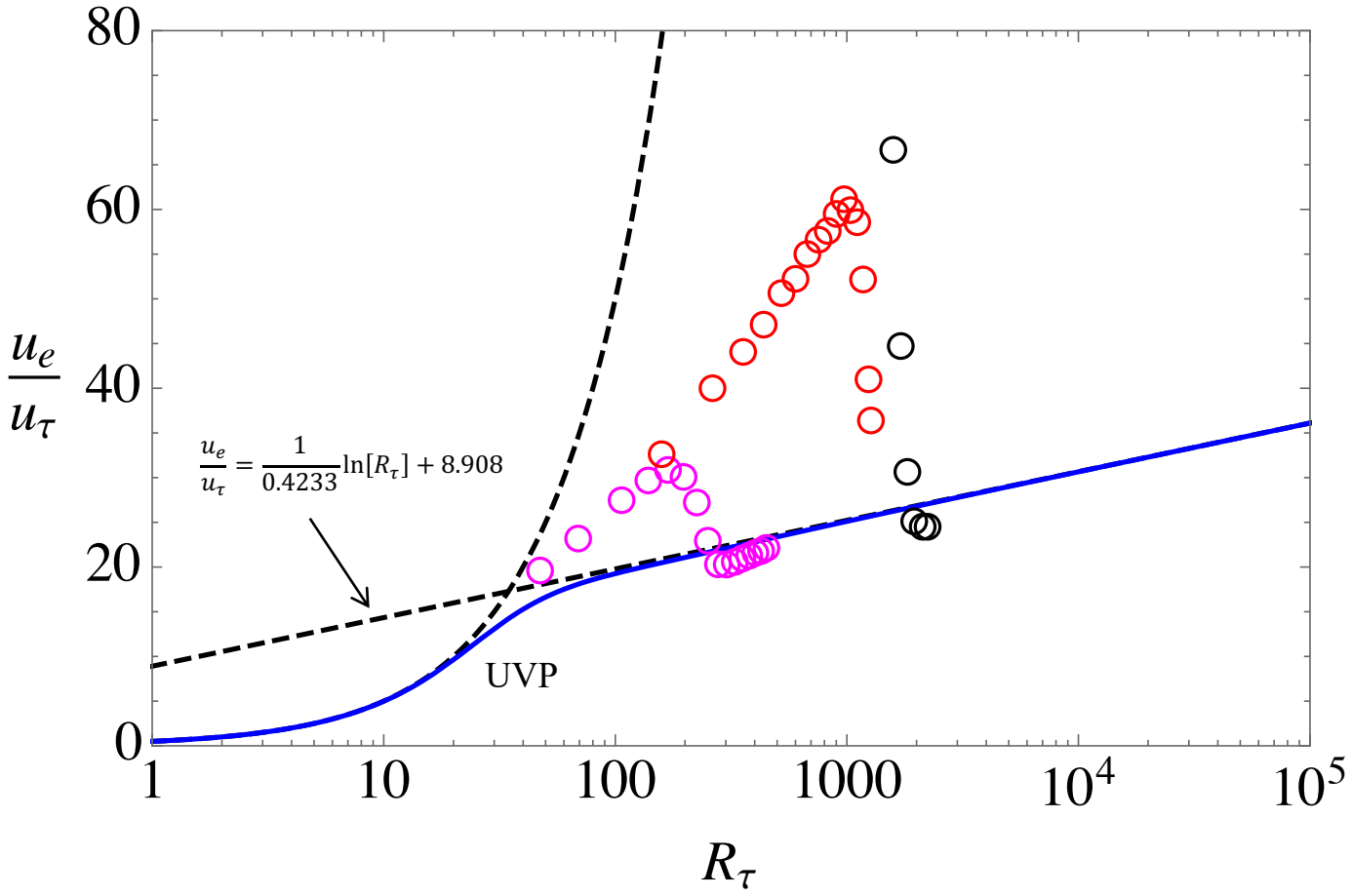

The laminar-turbulent transition inherent to the UVP is that of a fully tripped boundary layer.

FIG. 9. The universal velocity profile friction law for a zero pressure gradient boundary layer along with transitional friction data from Schubauer and Klebanoff[30] (natural transition $T_u = 0.03\%$—black) and Coupland[31] (ERCOFTAC case T3A $T_u = 0.9\%$—red, case T3A $T_u = 3.0\%$—magenta).

STANFORD
AERONAUTICS & ASTRONAUTICS

Recall the UVP

$$u^+(k,a,m,b,n,R_\tau,y^+) = \int_0^{y^+} \frac{2\left(1-\frac{s}{R_\tau}\right)}{1+\left(1+4\lambda^2\left(1-\frac{s}{R_\tau}\right)\right)^{1/2}} ds$$

$$\lambda(k,a,m,b,n,R_\tau,y^+) = \frac{ky^+(1-e^{-(y^+/a)^m})}{\left(1+\left(\frac{y^+}{bR_\tau}\right)^n\right)^{1/n}}$$

Carry out a scaling - Multiply and divide the damping and wake terms by *k*

Modified wall-wake mixing length function. The parameters *k* and *a* become one parameter *ka*.

$$\lambda(k,a,m,b,n,R_\tau,y^+) = \frac{ky^+(1-e^{-(y^+/a)^m})}{\left(1+\left(\frac{y^+}{bR_\tau}\right)^n\right)^{1/n}} = \frac{ky^+(1-e^{-(ky^+/ka)^m})}{\left(1+\left(\frac{ky^+}{bkR_\tau}\right)^n\right)^{1/n}} = \tilde{\lambda}(ka,m,b,n,kR_\tau,ky^+)$$

$y^+ \rightarrow ky^+$

$R_\tau \rightarrow kR_\tau$

Scaled velocity profile

$$ku^+(ka,m,b,n,kR_\tau,ky^+) = \int_0^{ky^+} \frac{2\left(1-\frac{s}{kR_\tau}\right)}{1+\left(1+4\tilde{\lambda}^2\left(1-\frac{s}{kR_\tau}\right)\right)^{1/2}} ds$$

$u/u_\tau \rightarrow ku/u_\tau$

Recall the shape function

$$\Phi(ka, m, b, n, kR_\tau, ky^+) = \int_0^{ky^+} \frac{2\left(1 - \frac{s}{kR_\tau}\right)}{1 + \left(1 + 4\tilde{\lambda}^2\left(1 - \frac{s}{kR_\tau}\right)\right)^{1/2}} ds - ln(ky^+)$$

Note $\quad ky^+ = \left(\frac{y}{\delta_h}\right) kR_\tau$

STANFORD
AERONAUTICS &
ASTRONAUTICS

Fix y/δ_h and plot Φ versus kR_τ

Above $kR_\tau \cong 2000$, Φ *is independent of* R_τ

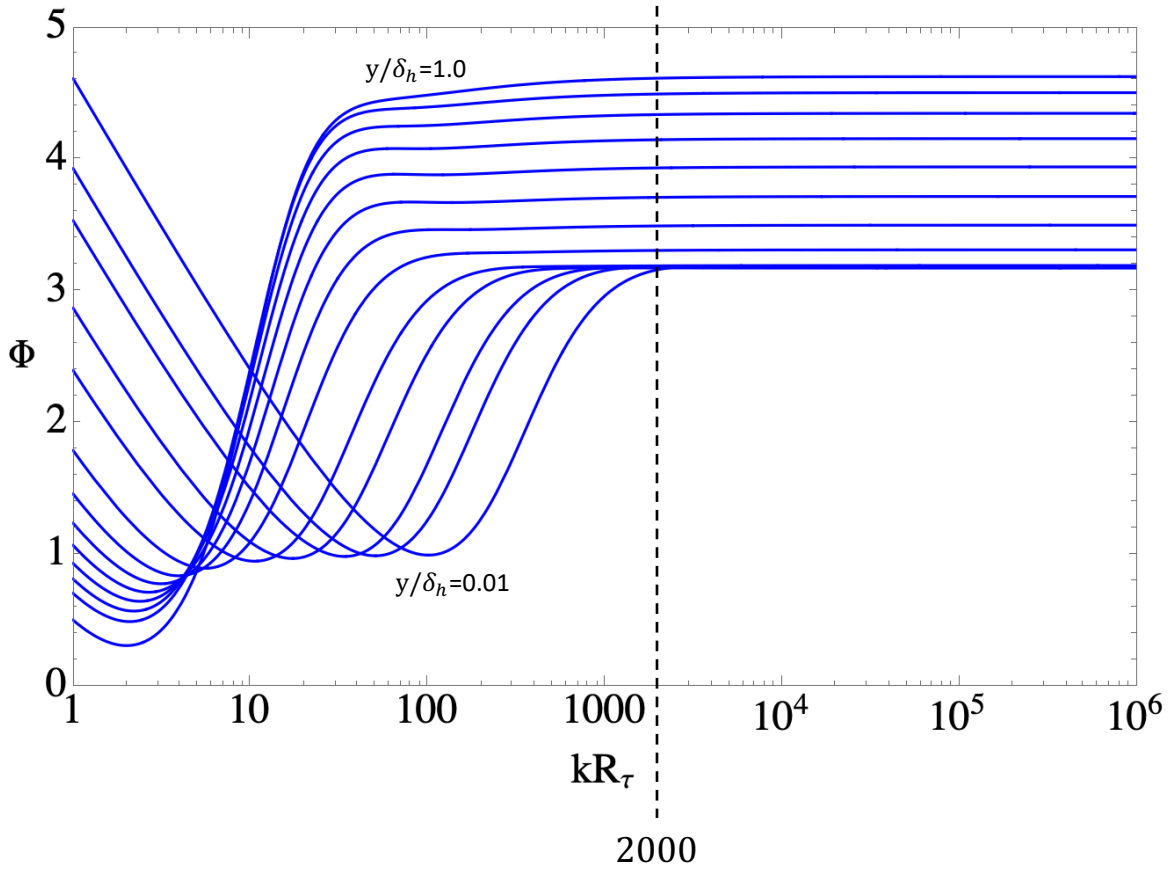

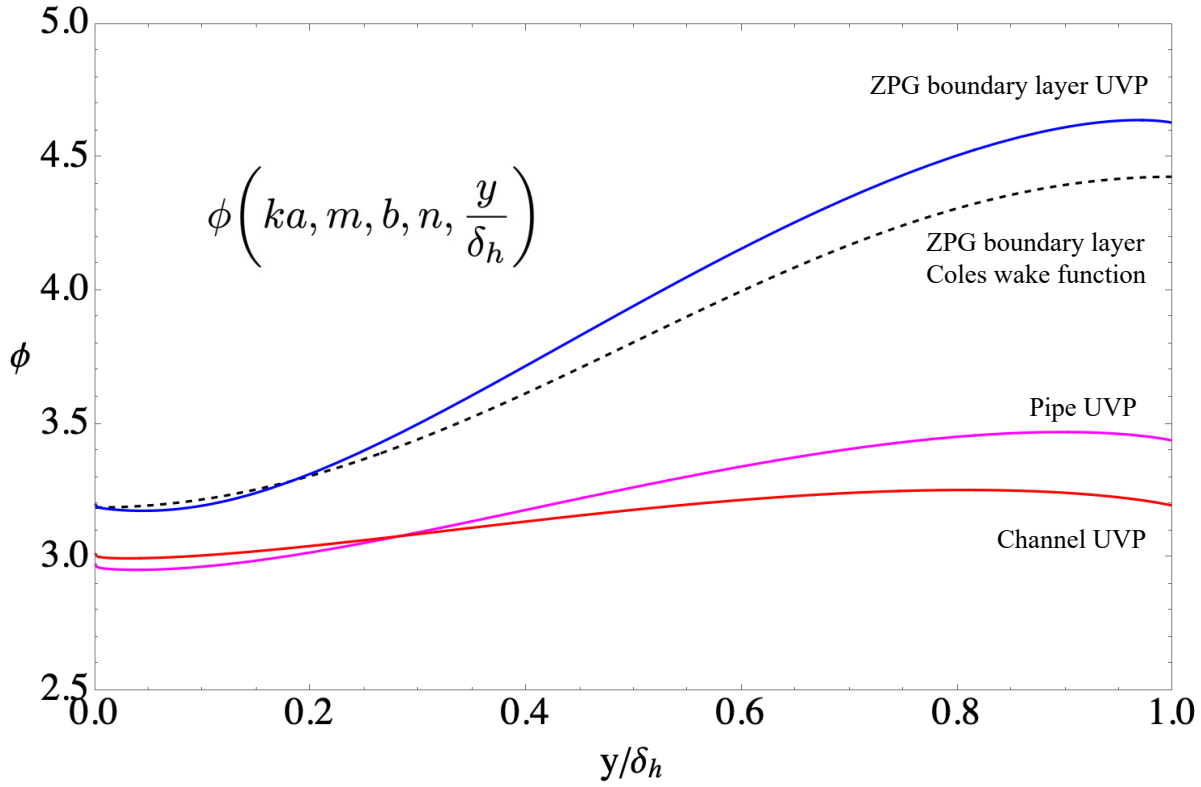

STANFORD
AERONAUTICS & ASTRONAUTICS

Explicit high Reynolds number form of the UVP

$$u^+(k,a,m,b,n,R_\tau,y^+) = \int_0^{y^+} \frac{2\left(1-\frac{s}{R_\tau}\right)}{1+\left(1+4\lambda^2\left(1-\frac{s}{R_\tau}\right)\right)^{1/2}} ds$$

$0 < y^+ < R_\tau$

At Reynolds numbers larger than $kR_\tau \cong 2000$ the boundary layer velocity profile above $y^+ = 132$ is accurately approximated by

$$u^+ = \frac{1}{k} ln(ky^+) + \frac{1}{k}\phi\left(ka, m, b, n, \frac{y}{\delta_h}\right)$$

$y^+ > 132$

Evaluate at the boundary layer edge to determine the friction law.

$$\frac{u_e}{u_\tau} = \frac{1}{k} ln(kR_\tau) + \frac{1}{k}\phi\left(ka, m, b, n, 1\right)$$

STANFORD
AERONAUTICS & ASTRONAUTICS

The UVP wake parameters *b* and *n* are detemined by β_c

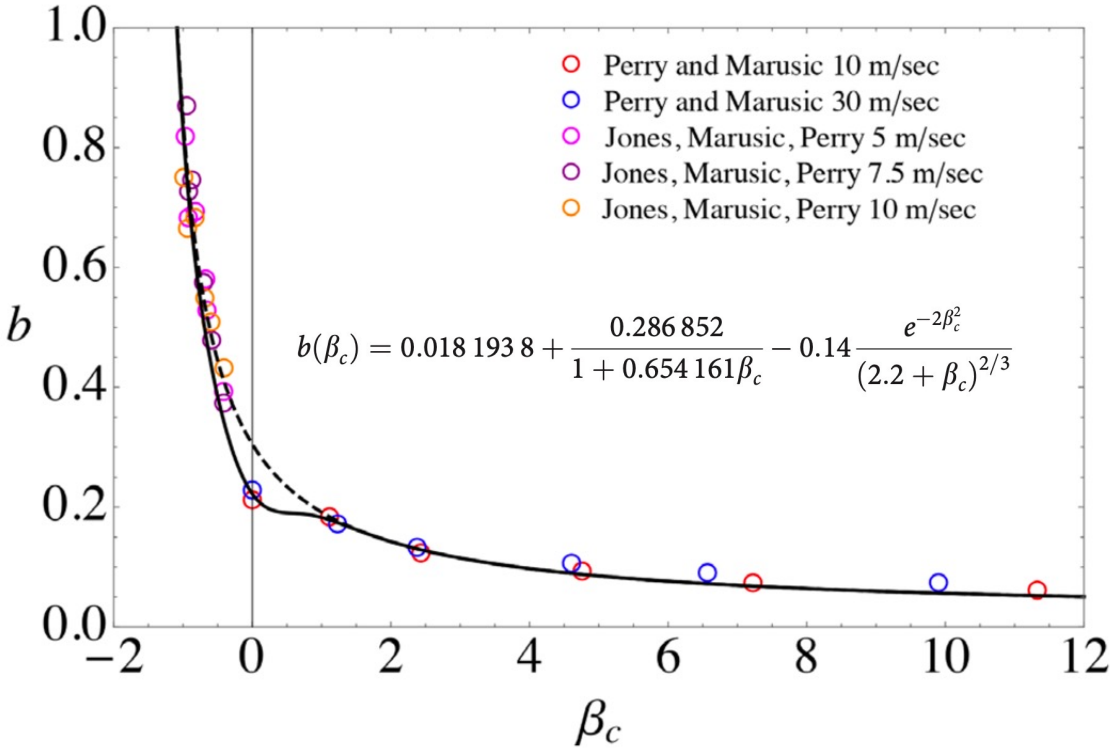

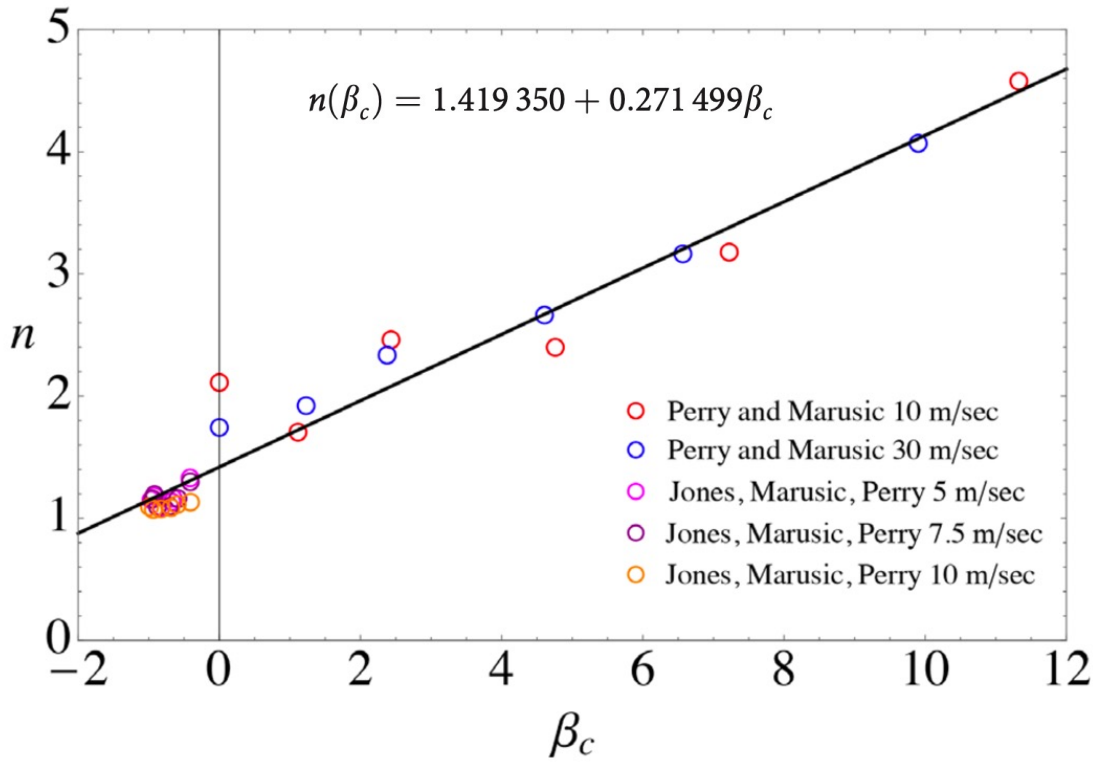

STANFORD
AERONAUTICS &
ASTRONAUTICS

The shape function for various β_c

$$u^+ = \frac{1}{k} ln(ky^+) + \frac{1}{k}\phi\left(ka, m, \beta_c, \frac{y}{\delta_h}\right)$$

$y^+ > 132$
$kR_\tau > 2000$

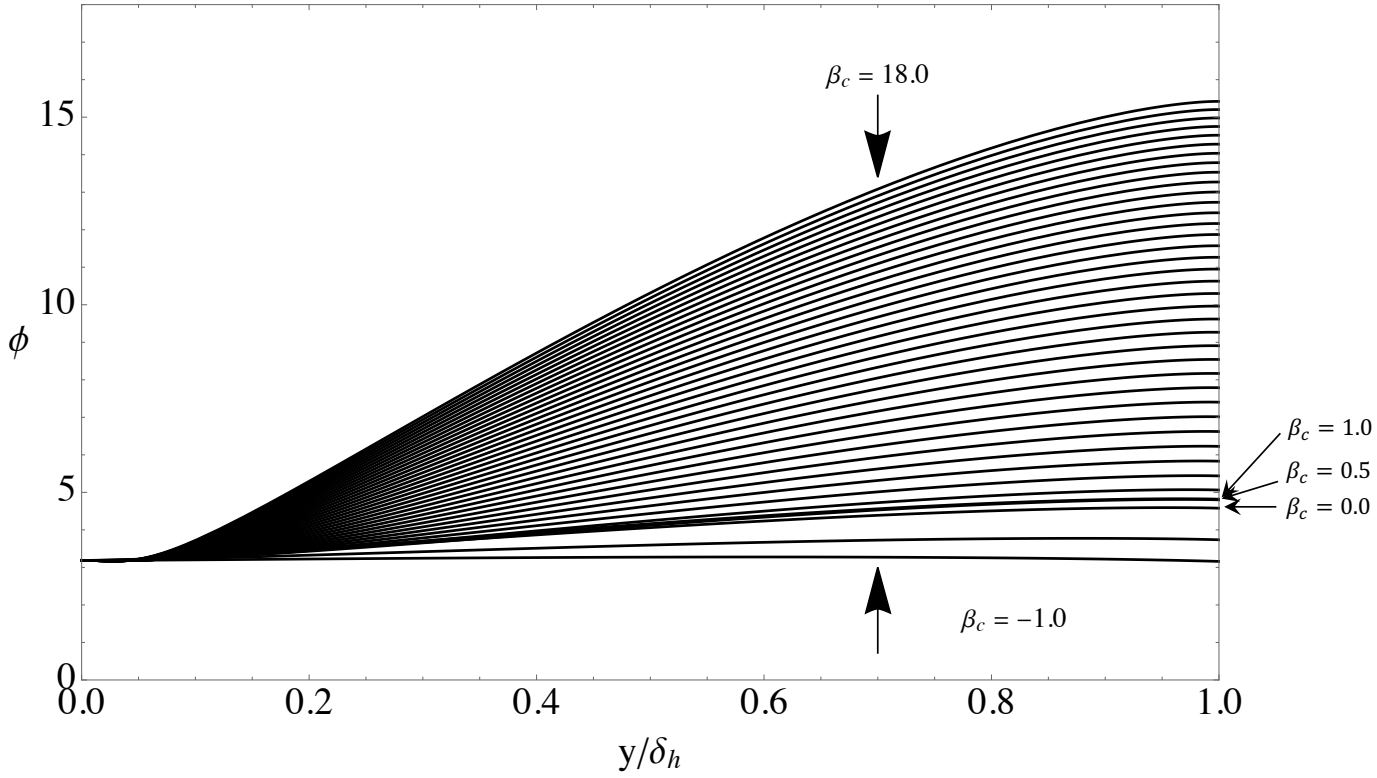

STANFORD AERONAUTICS & ASTRONAUTICS

The shape function is accurately approximated by a bivariate polynomial in β_c and y/δ_h.

In the presence of a pressure gradient, the wall parameters (*k, a, m*) are kept constant at the ZPG boundary layer values while the wake parameters (*b, n*) are treated as functions of β_c using the correlations. The figure at the right shows the shape function for a range of values of β_c. Changes in ϕ with β_c are smooth and monotonic. A polynomial of high order is a safe, reliable fit in this situation since there is no question of y/δ_h falling outside of the range $0 \le y/\delta_h \le 1$. The family of shape functions shown in the Figure is accurately approximated by an eighth-order polynomial.

$$\phi\left(\beta_c, \frac{y}{\delta_h}\right) = c_0(\beta_c) + c_1(\beta_c)\left(\frac{y}{\delta_h}\right) + c_2(\beta_c)\left(\frac{y}{\delta_h}\right)^2 + c_3(\beta_c)\left(\frac{y}{\delta_h}\right)^3 + c_4(\beta_c)\left(\frac{y}{\delta_h}\right)^4 + c_5(\beta_c)\left(\frac{y}{\delta_h}\right)^5 + c_6(\beta_c)\left(\frac{y}{\delta_h}\right)^6 + c_7(\beta_c)\left(\frac{y}{\delta_h}\right)^7 + c_8(\beta_c)\left(\frac{y}{\delta_h}\right)^8$$

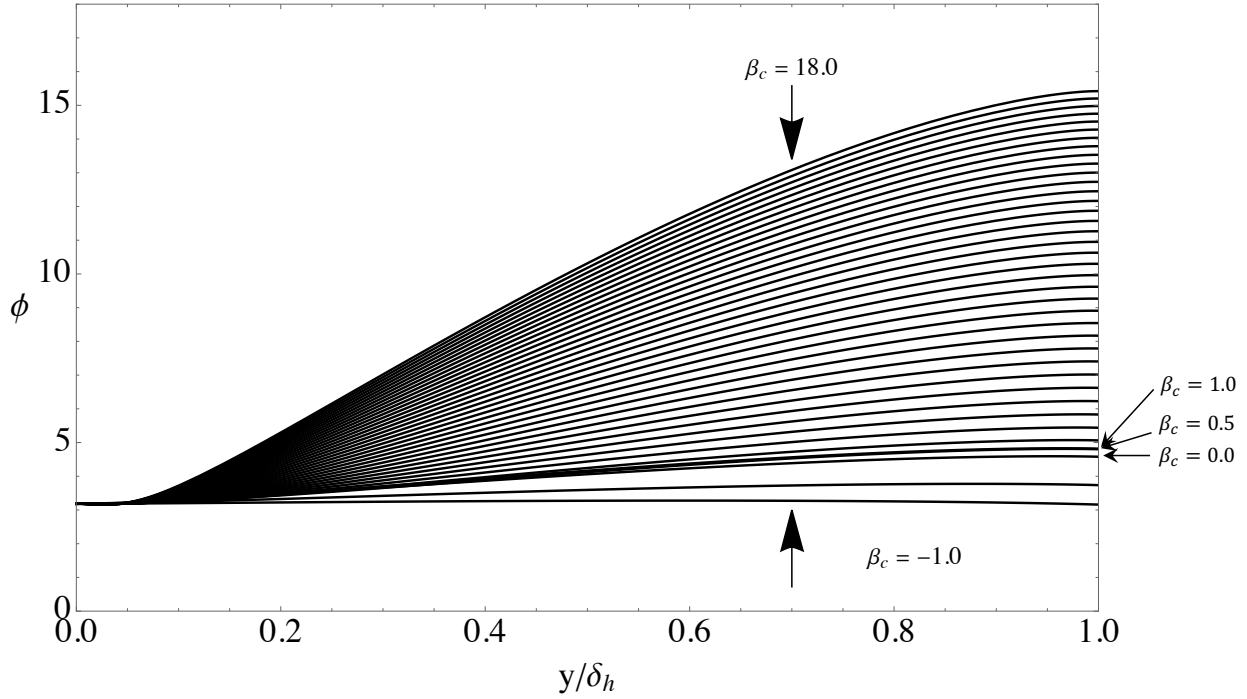

It is important to note that $\phi(\beta_c, y/\delta_h)$ is universal in the sense that it applies to any pressure gradient wall flow that falls in the range -1 < β_c < 18. Higher order fits could be used to increase the range of β_c beyond 18.0.

With $\phi(ka, m, \beta_c, y/\delta_h)$ known explicitly as a bivariate polynomial, the displacement thickness and momentum thickness integrals can be carried out up to whatever R_τ is required. This leads to polynomial expressions for the friction and thickness functions $F_0(\beta_c, R_\tau)$, $F_1(\beta_c, R_\tau)$, $F_2(\beta_c, R_\tau)$ and $F_3(\beta_c, R_\tau)$. Once these functions are known, the UVP integral method no longer requires the computation of nested integrals. As a result, the time to calculate a solution of the Karman integral equation is independent of the Reynolds number. The viscous drag coefficient for any chord Reynolds number airfoil can be determined in a few seconds. Above about R_{chord} = 10^6, the explicit UVP method matches the results using the integral form of the UVP almost exactly.

Boundary layer integrals in terms of the UVP

$R_\tau < 2000/k$

$$u^+ = \int_0^{y^+} \frac{2\left(1-\frac{s}{R_\tau}\right)}{1+\left(1+4\lambda^2\left(1-\frac{s}{R_\tau}\right)\right)^{1/2}} ds$$

$$\frac{u_e}{u_\tau} = \int_0^{R_\tau} \frac{2\left(1-\frac{s}{R_\tau}\right)}{1+\left(1+4\lambda^2\left(1-\frac{s}{R_\tau}\right)\right)^{1/2}} ds \equiv F_0(\beta_c, R_\tau)$$

For R_τ < 2000/k, F_1, F_2 and F_3 require nested integration and can be relatively slow to evaluate.

$R_\tau > 2000/k$

$$u^+ = \frac{1}{k} ln(ky^+) + \frac{1}{k}\phi\left(ka, m, \beta_c, \frac{y}{\delta_h}\right)$$

$$\frac{u_e}{u_\tau} = \frac{1}{k} ln(R_\tau) + \frac{1}{k} ln(k) + \frac{1}{k}\phi\left(ka, m, \beta_c, 1\right) \equiv F_0(\beta_c, R_\tau)$$

$$R_{\delta_1} = \frac{u_e \delta_1}{\nu} = \frac{u_e}{u_\tau}\int_0^{R_\tau}\left(1-\frac{u_\tau}{u_e}u^+\right) dy^+ \equiv F_1(\beta_c, R_\tau)$$

$$R_{\delta_2} = \frac{u_e \delta_2}{\nu} = \int_0^{R_\tau} u^+\left(1-\frac{u_\tau}{u_e}u^+\right) dy^+ \equiv F_2(\beta_c, R_\tau)$$

$$\frac{dF_2}{dR_\tau} \equiv F_3(\beta_c, R_\tau)$$

For R_τ > 2000/k F_0, F_1, F_2 and F_3 are known explicitly as algebraic and logarithmic functions of β_c and R_τ and can be evaluated quickly at <u>any</u> Reynolds number.

STANFORD AERONAUTICS & ASTRONAUTICS

Use the Kármán integral equation to relate R_τ to $\xi = x/r$.

$$\frac{d\delta_2}{dx} + (2\delta_2 + \delta_1)\frac{1}{u_e}\frac{du_e}{dx} - \left(\frac{u_\tau}{u_e}\right)^2 = 0$$

$$\beta_c = \frac{\delta_1 + \delta_2}{\tau_w}\frac{dp_e}{ds}$$

$$\frac{dR_\tau}{d\xi} = \frac{UR_e}{{F_0}^2 F_3}\left(1 - \frac{{F_0}^2}{R_e}(F_2 + F_1)\frac{1}{U^2}\frac{dU}{d\xi}\right)$$

$$\beta_c = -\frac{{F_0}^2}{R_e}(F_2 + F_1)\frac{1}{U^2}\frac{dU}{d\xi}$$

$$\frac{dR_\tau}{d\xi} = \frac{UR_e}{{F_0}^2 F_3}(1 + \beta_c)$$

Use β_c to adjust *b* and *n* at each streamwise point.

Assume the boundary layer wall parameters (k, a, m) do not depend on the pressure gradient.

Potential flow velocity distributions about the J0012 and NACA 0012 airfoils

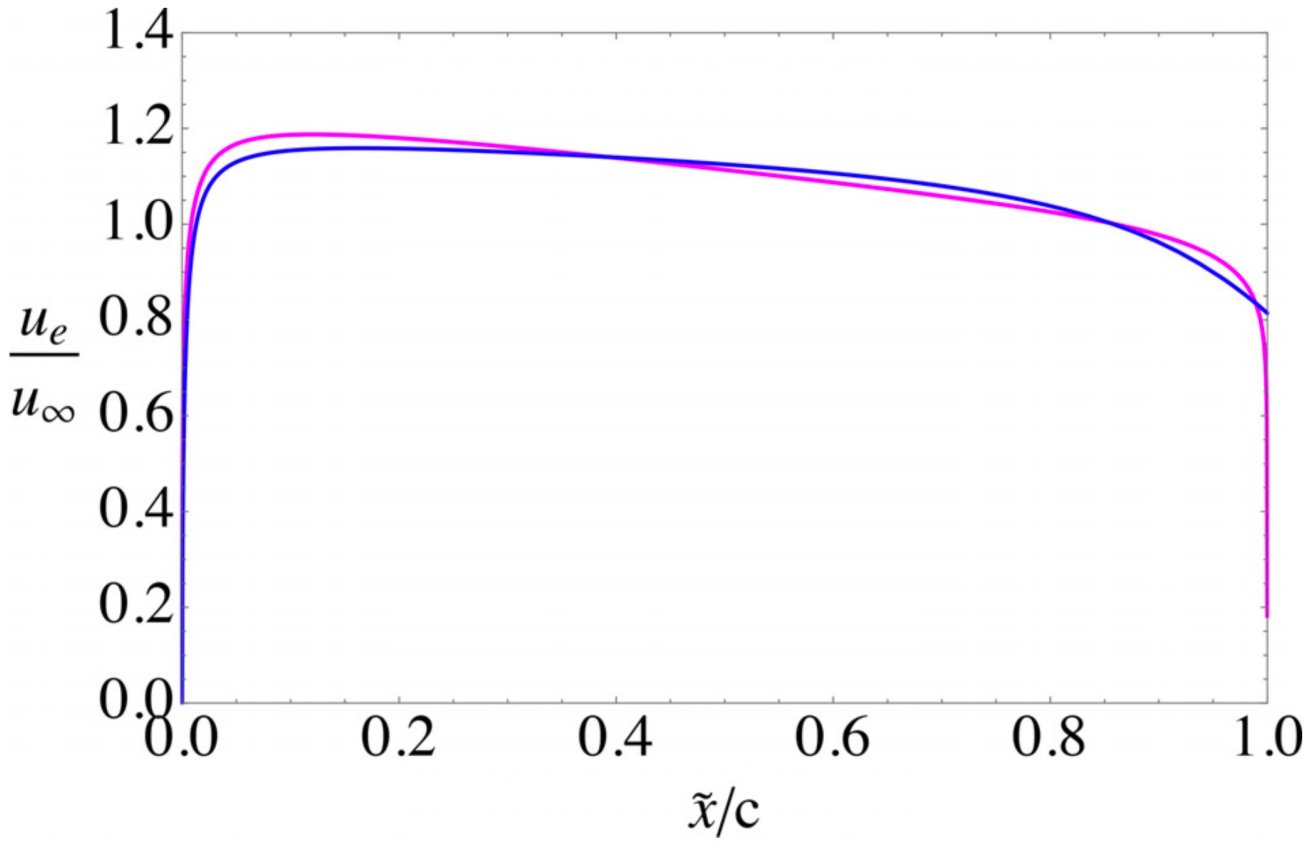

FIG. 24. Potential flow velocity distributions about the J0012 (blue) and NACA0012 (magenta) airfoils.

Integration procedure

1) The first iteration uses the UVP with the constants (*k*, *a*, *b*, *m*, *n*) fixed at the ZPG values (β_c = 0) to determine the initial distribution of $R_{\tau 1}(\xi)$.

2) $R_{\tau 1}(\xi)$ is then used to prepare for iteration 2. The UVP is used to compute F0, F1, F2, F3 and β_c at each point over the airfoil. The β_c distribution is used determine the UVP parameters b($R_\tau(\xi)$) *and* n($R_\tau(\xi)$). The wall parameters (*k*, *a*, *m*) remain fixed at the ZPG values. This data is used to solve for the next iteration $R_{\tau 2}$(x/r).

3) The process is repeated until the ith iterate when $R_{\tau i}(\xi)$ no longer changes.

4) $U(\xi)$ can be updated using the airfoil+displacement thickness to recalculate the potential flow. This does not change the viscous drag measurably for the cases considered.

STANFORD
AERONAUTICS &
ASTRONAUTICS

Iterations J0012

$Re_{chord} = 10^7$

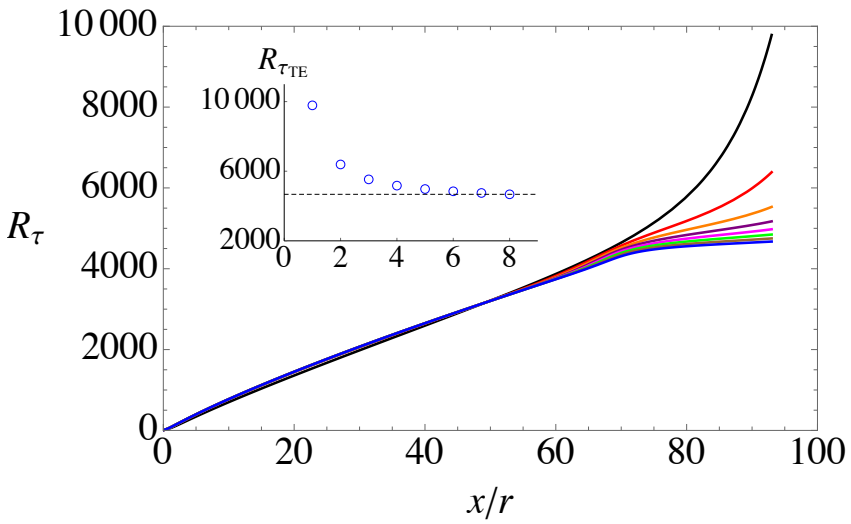

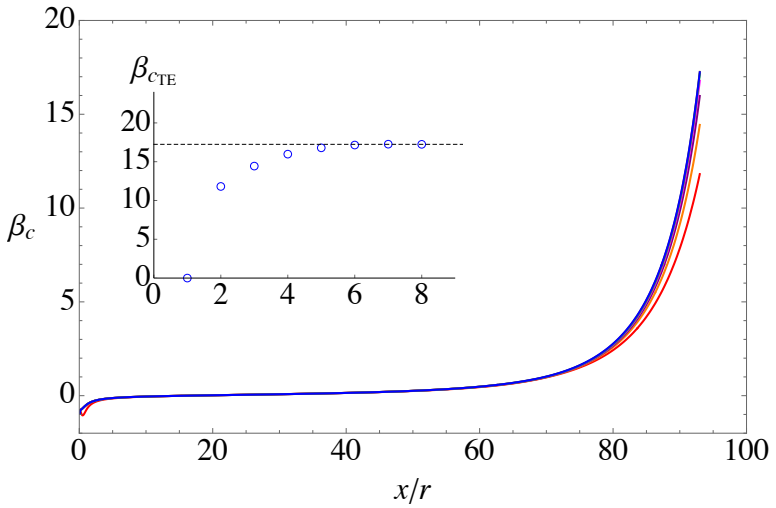

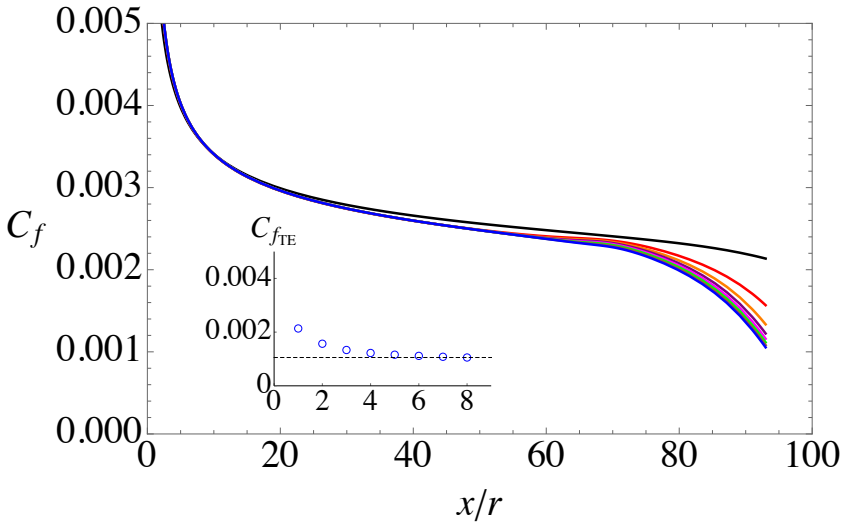

STANFORD
AERONAUTICS &
ASTRONAUTICS

Iterations J0012, cont'd

$Re_{chord} = 10^7$

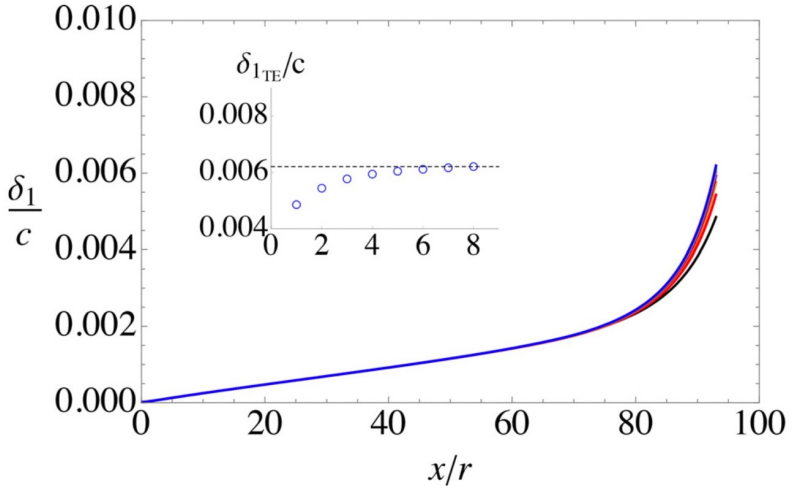

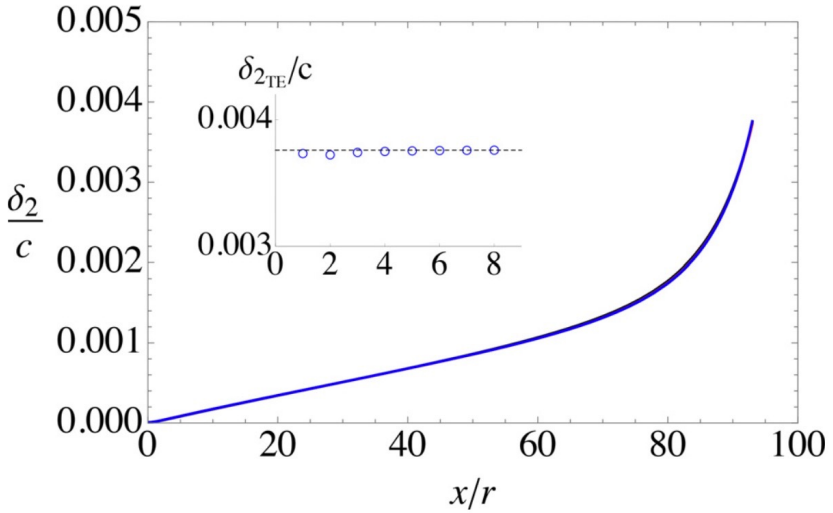

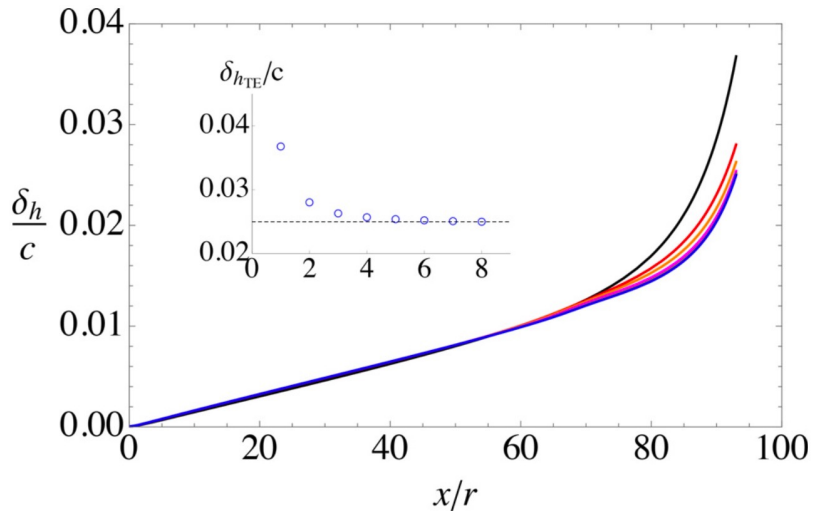

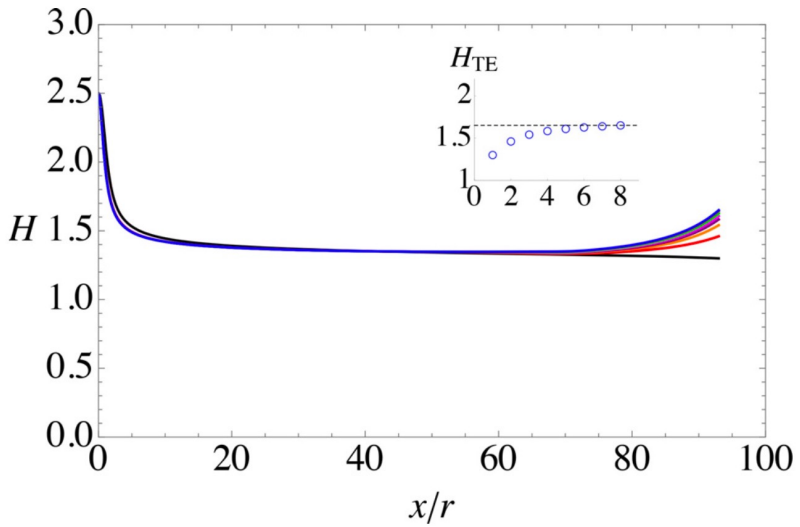

Iterations J0012, cont'd

$Re_{chord} = 10^7$

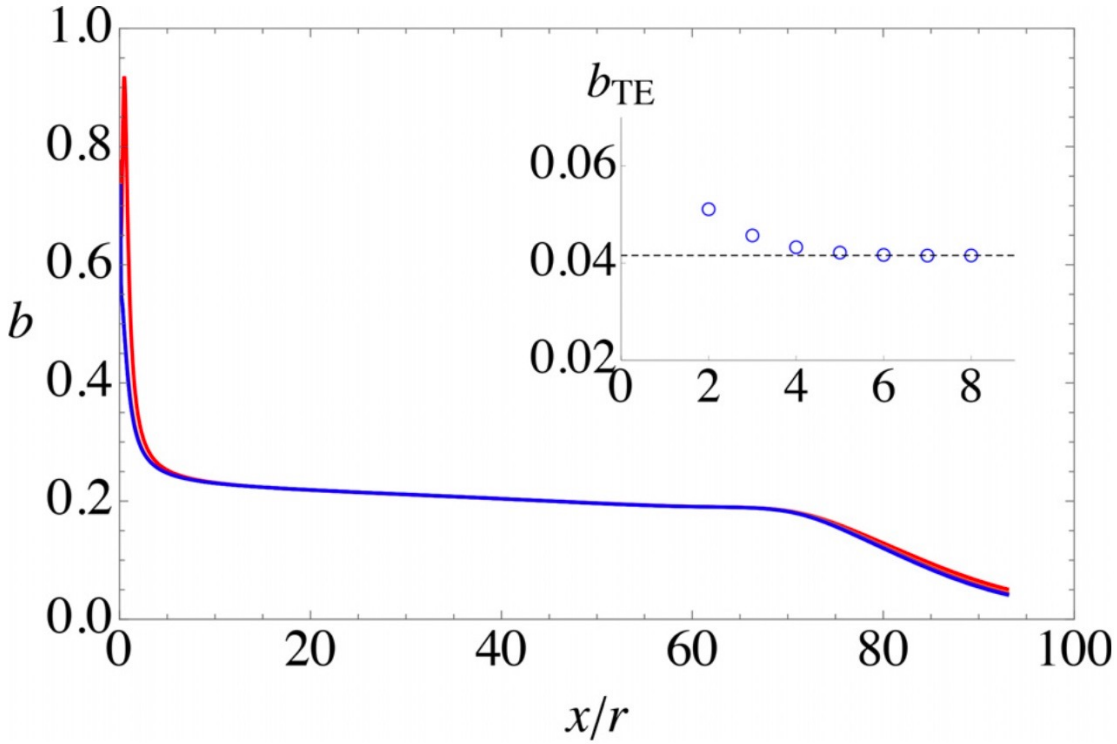

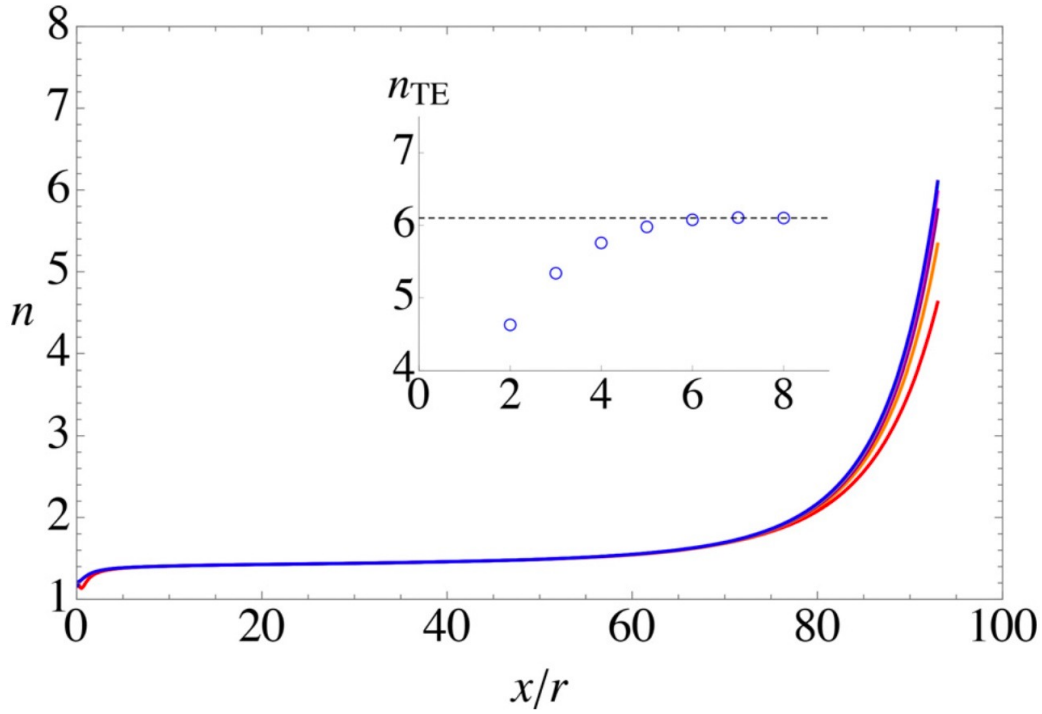

STANFORD
AERONAUTICS &
ASTRONAUTICS

Viscous drag coefficient convergence

$$C_{d_v} = \frac{D_v}{\frac{1}{2}\rho {u_\infty}^2 c} = 2\int_0^1 \left(\frac{u_e}{u_\infty}\right)^2 C_f d\left(\frac{\tilde{x}}{c}\right)$$

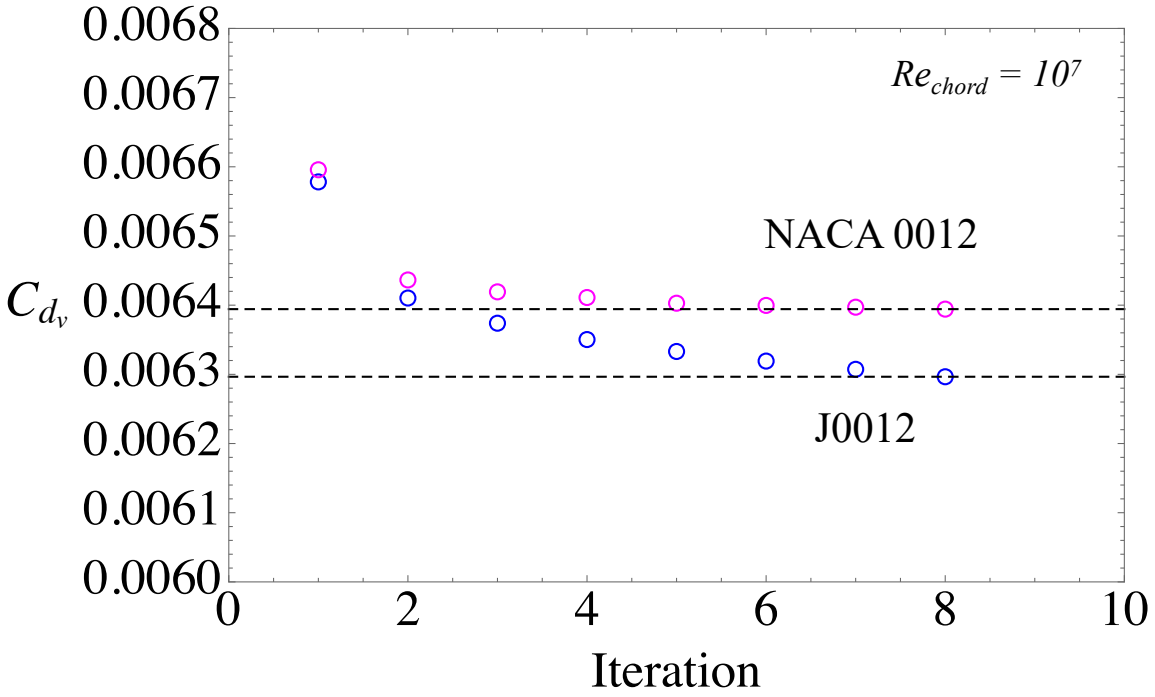

STANFORD
AERONAUTICS &
ASTRONAUTICS

Main Results - Viscous drag coefficient

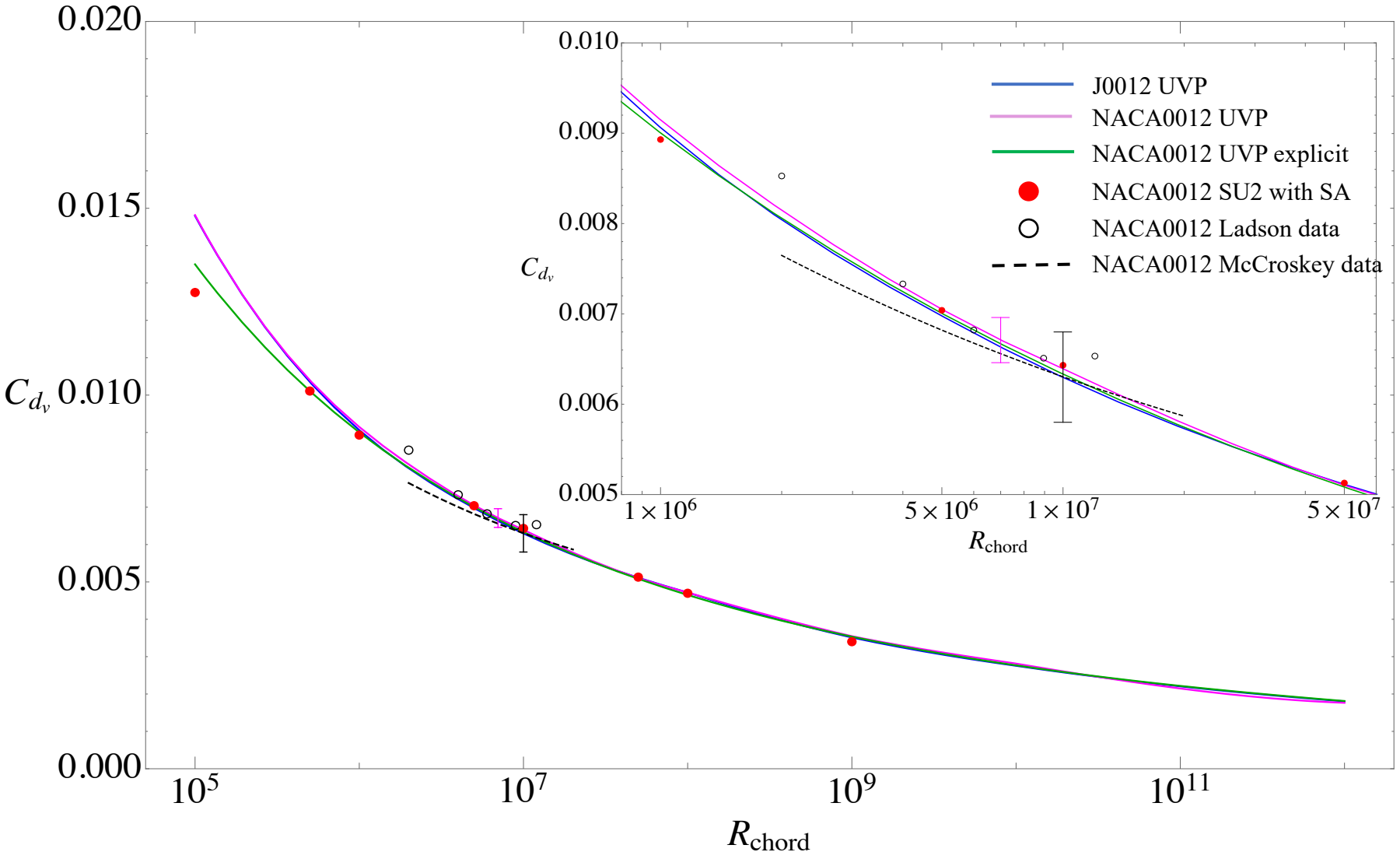

Rough-wall pipe flow

Rough-wall pipe velocity profile

$$u_r^+(R_\tau, h^+, y^+) = u^+(R_\tau, y^+) - \Delta u_r^+(h^+)$$

Where $u^+(R_\tau, y^+)$ is the smooth-wall UVP.

The Clauser roughness velocity is

$$\Delta u_r^+(h^+) = \frac{1}{k} f(h^+) ln(1 + \alpha h^+)$$

The roughness fraction of the smooth-wall Princeton Super Pipe is $\varepsilon = 6.96 \times 10^{-6}$.
At the highest PSP Reynolds number, h+ = 3.69 indicating that the entire data set is hydraulically smooth except possibly for a very small effect at the highest Reynolds number.

Roughness height Reynolds number, roughness fraction

$$h^+ = \frac{h_s u_\tau}{\nu} \qquad \varepsilon = \frac{h_s}{R} = \frac{h^+}{R_\tau}$$

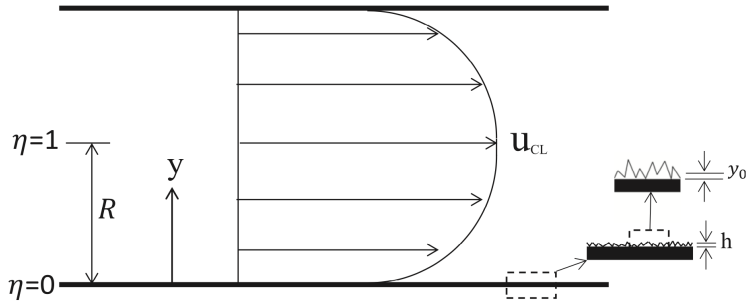

FIG. 1. Rough-wall pipe flow with nomenclature.

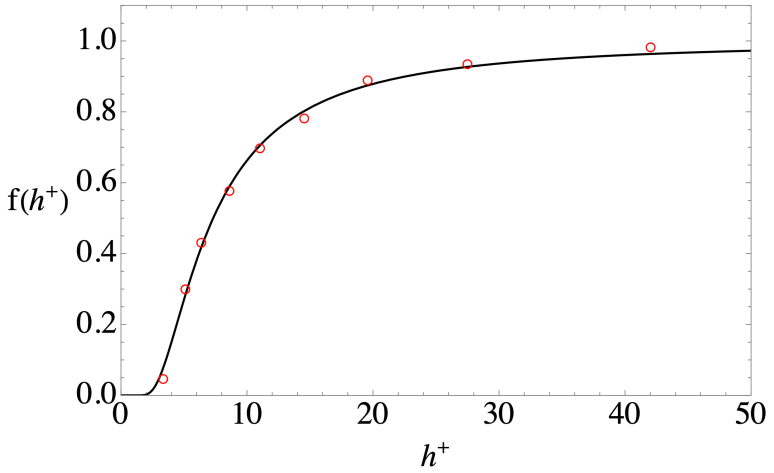

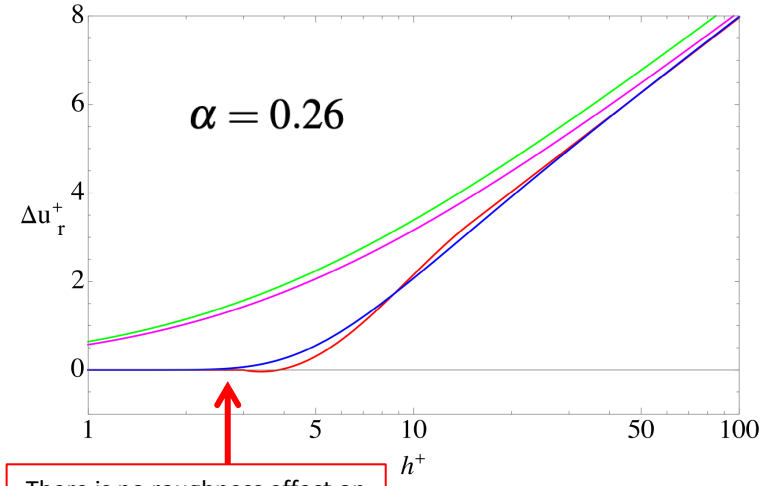

There is no roughness effect on pipe friction below h+ = 3.5

Comparison of UVP roughness function (blue) with other commonly used functions: Nikuradse (red), White (green) and Grigson (magenta).

STANFORD AERONAUTICS & ASTRONAUTICS

UVP fit to Rough-wall Princeton Super Pipe experimental data, $R_\tau = 28800\ to\ 361000$

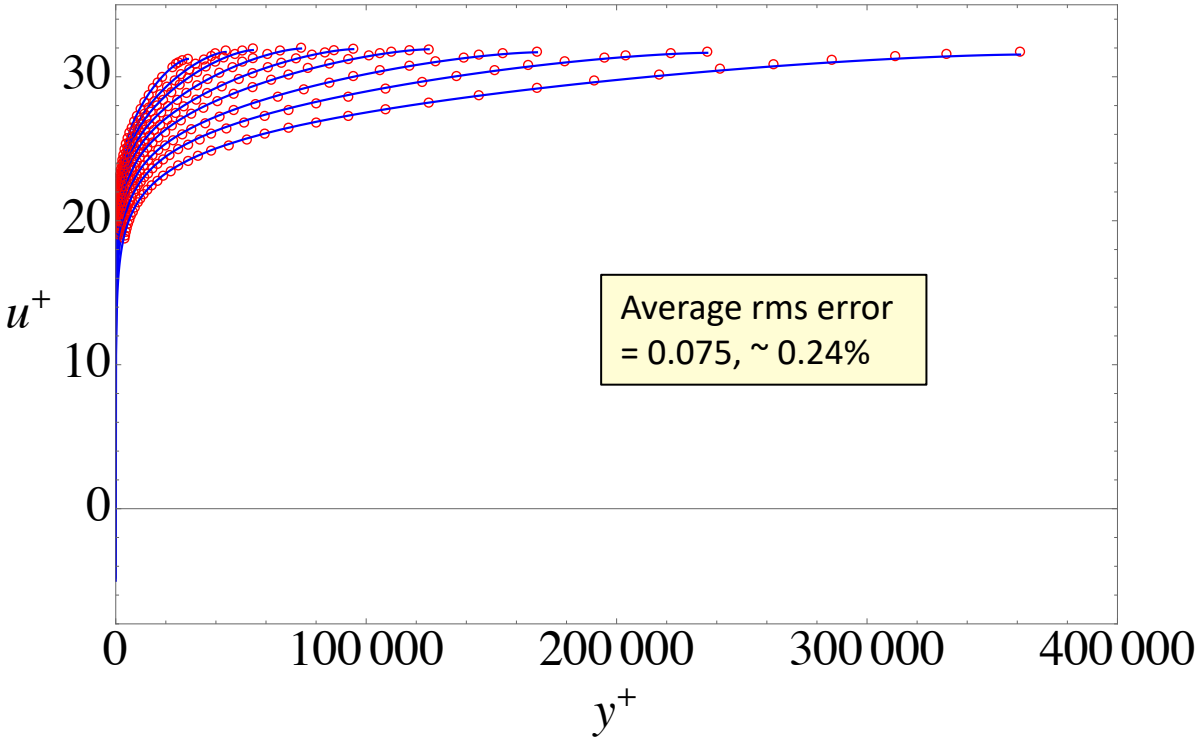

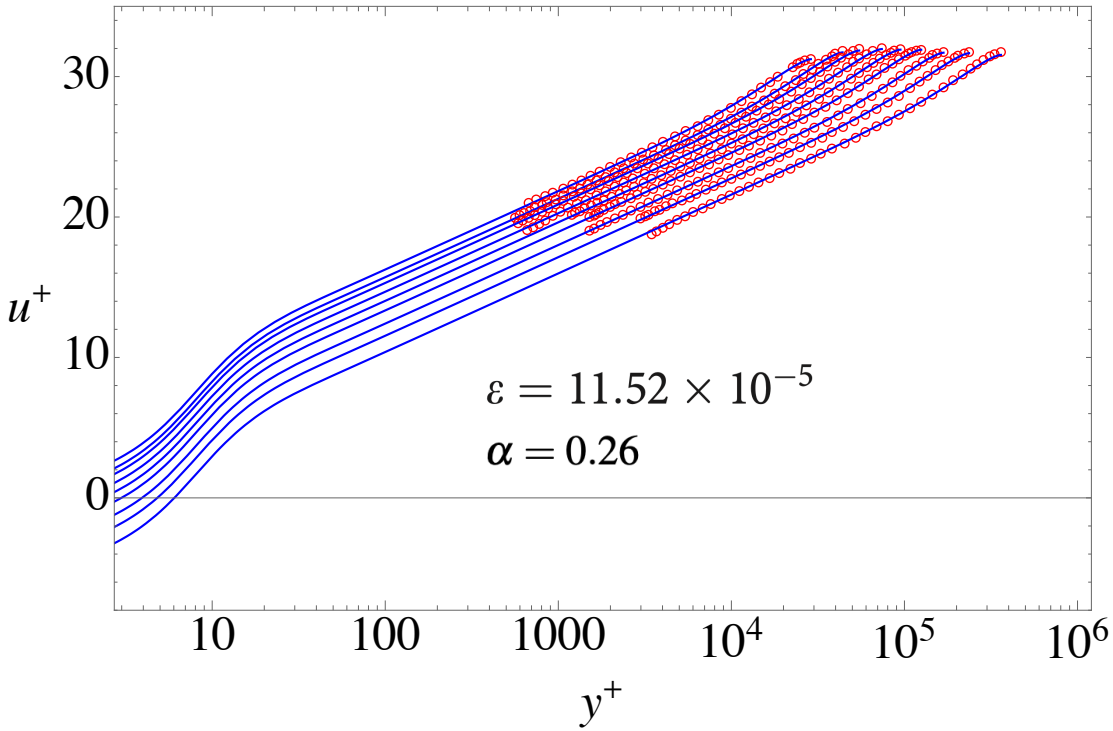

TABLE I. Average model parameters with standard deviation for basic wall flows. Ranges of R_τ for each flow are as follows: Pipe (3327–530 023), Channel (550–8016), ZPG boundary layer (1343–17 207).

Flow	$\bar{k}$	σ_k	$\bar{a}$	σ_a	$\bar{m}$	σ_m	$\bar{b}$	σ_b	$\bar{n}$	σ_n
Pipe (21 profiles)	0.4092	0.0057	20.0950	0.381	1.6210	0.0379	0.3195	0.0157	1.6190	0.1204
Channel (7 profiles)	0.4086	0.0179	22.8673	1.599	1.2569	0.0292	0.4649	0.0485	1.3972	0.1213
ZPG boundary layer (11 profiles)	0.4233	0.0068	24.9583	0.663	1.1473	0.0373	0.1752	0.0060	2.1707	0.2238

STANFORD
AERONAUTICS & ASTRONAUTICS

Fraction of the sand-grain roughness height where the velocity goes to zero

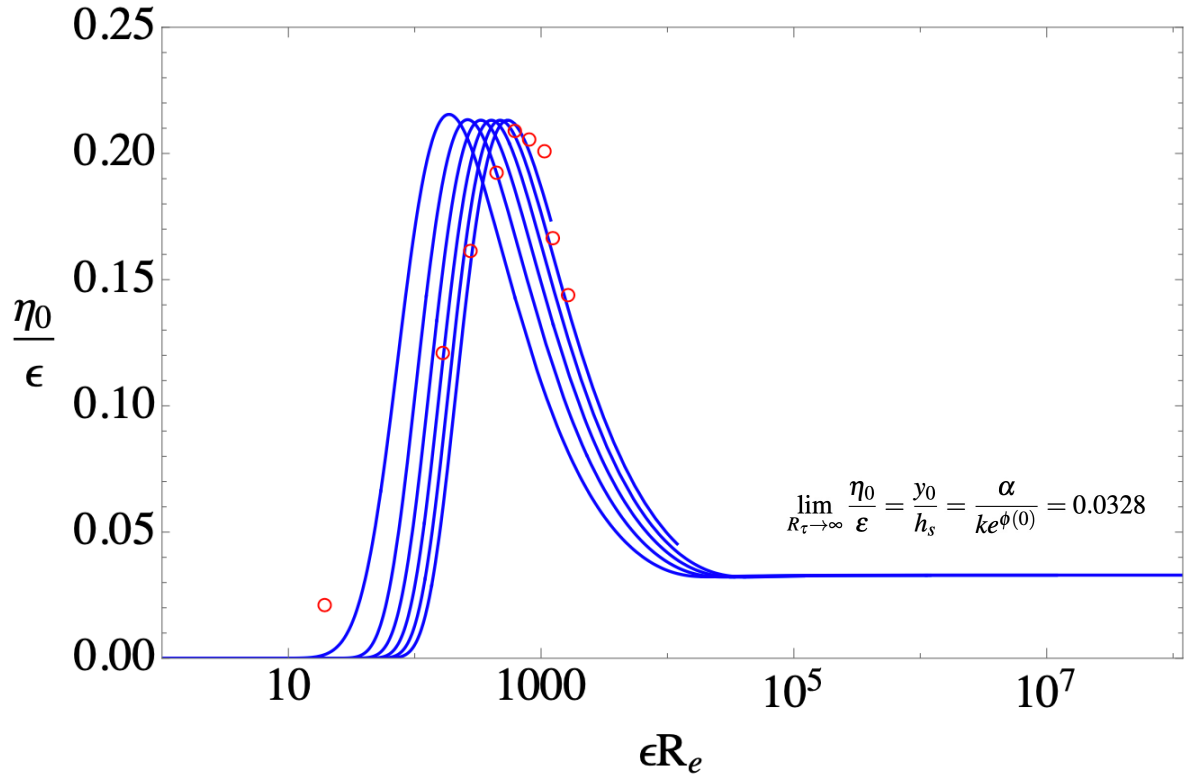

FIG. 12. Fraction of the sand-grain roughness height near the wall where the velocity is zero, η_0/ε, versus εRe for $\varepsilon = 0.1, 0.01, 0.001, 0.0001, 0.00001, 0.000001$ from left to right. Red open discs are generated from data in Table II.

The Princeton rough-wall pipe experiments do not represent an asymptotically rough wall despite the very large Reynolds number.

STANFORD
AERONAUTICS &
ASTRONAUTICS

Revised pipe flow Moody diagram

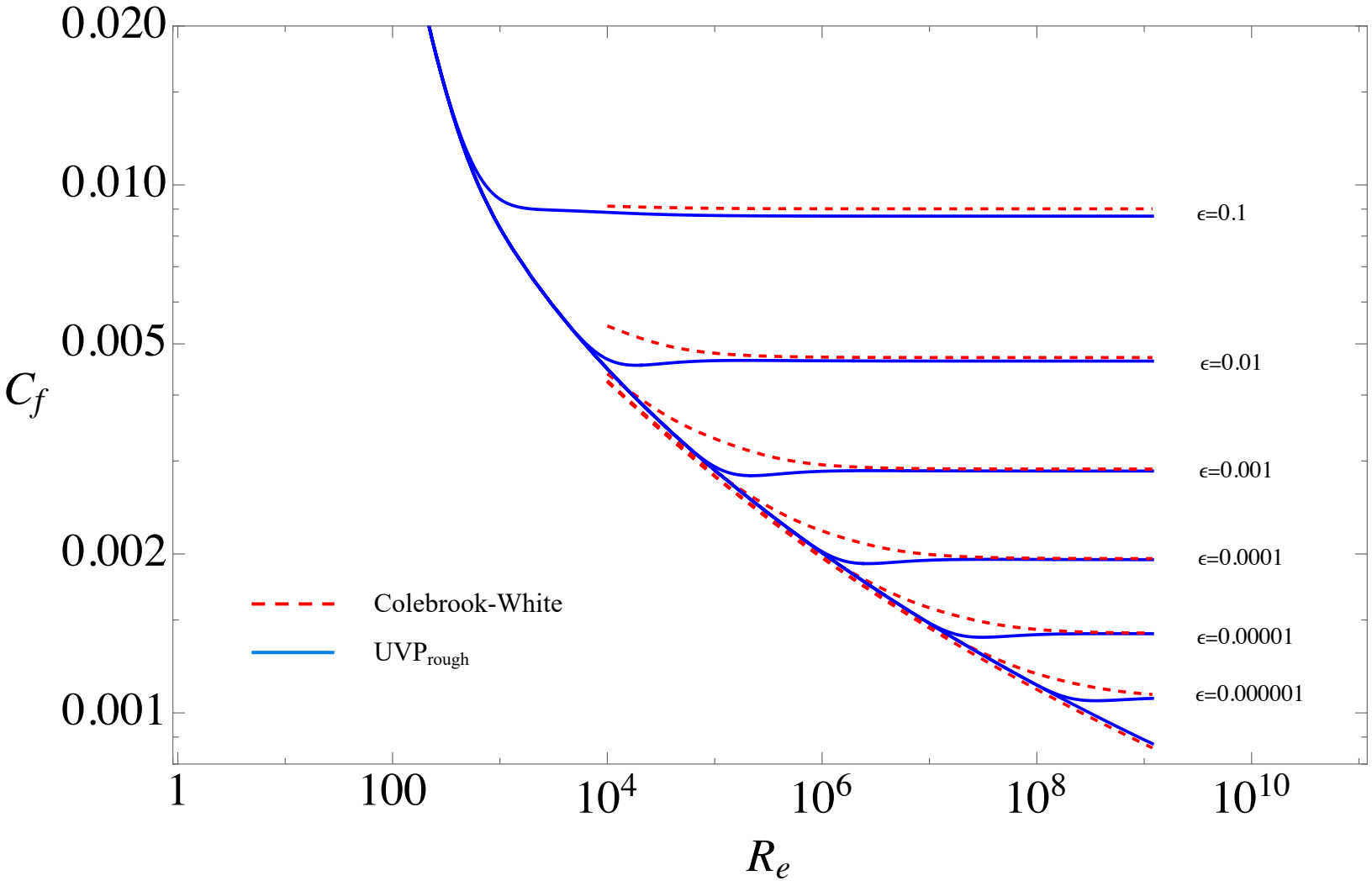

STANFORD
AERONAUTICS &
ASTRONAUTICS

Conclusions

1) A modified Clauser parameter, β_c, is shown to correlate well with the parameters *b* and *n* that characterize the wake portion of the UVP. This result allows a complete characterization of the Reynolds number and pressure gradient dependence of the UVP.

2) The inherent dependence of the UVP on Reynolds number, extended to include the effect of pressure gradient enables it to be used as the basis of a new method for integrating the Karman equation for a wide variety of attached, wall bounded flows. There is really no practical limit to the Reynolds number that can be evaluated suggesting that, with modification for the effects of compressibility and/or roughness, the method can be applied to very large-scale aerodynamic, hydrodynamic, and geophysical flows.

3) With the model parameters held fixed, the smooth-wall UVP together with a new roughness transition function and the Clauser roughness velocity function approximates Princeton rough-wall pipe data to a high level of accuracy commensurate with the smooth wall case.

4) The point where the rough wall velocity profile is zero is found to be no more than 20% of the sand-grain roughness height

5) For εRe > 30 000, y_0 is a little more than 3% of the sand grain height. Laboratory experiments are likely to be below this range, unless the roughness fraction and/or Reynolds number are very large. This means that an asymptotically rough wall is essentially out of reach of current experiments.

6) In aggreement with She et al (2012), details such as the inflectional shape in the friction law in the transitionally rough regime, are accurately captured by the rough UVP friction law providing improved accuracy over a wide range of roughness fractions and Reynolds numbers.

STANFORD AERONAUTICS & ASTRONAUTICS

Main References

Coles, D.E. 1956 The law of the wake in the turbulent boundary layer. *J. Fluid Mech.* 1 (2), 191–226.

Prandtl, L. 1934 *Aerodynamic Theory* (ed. W. F. Durand), vol III, chap. 21, p. 134. Julius Springer.

Cantwell, B.J. 2019 A universal velocity profile for smooth wall pipe flow. *J. Fluid Mech.* 878, 834–874.

Spalding, B.D. 1961 A single formula for the 'law of the wall'. *Trans. ASME J. Appl. Mech.* 0, 455–458.

Cantwell, B.J. 2021 Integral measures of the zero pressure gradient boundary layer over the Reynolds number range $0 \leq R_T < \infty$. *Phys. Fluids* 33, 085108.

Cantwell, B. J., E. Bilgin, and J. T. Needels, "A new boundary layer integral method based on the universal velocity profile," Physics of Fluids 34, 075130 (2022).

Subrahmanyam, M. A., B. J. Cantwell, and J. J. Alonso, "A universal velocity profile for turbulent wall flows including adverse pressure gradient boundary layers,"JFM. 933, A16 (2022).

Bilgin, E., and B. Cantwell, 2023 Application of the Universal Velocity Profile to rough-wall pipe flow. Phys. Fluids 35, 055135.

Spalart, P. R., and S. R. Allmaras, "A one equation turbulence model for aerodynamic flows," AIAA Paper No. 89-0366, 1992.

Clauser, F. H., "Turbulent boundary layers in adverse pressure gradients," J. Aeronaut. Sci. 21, 91–108 (1954).

Van Dyke, M., Perturbation Methods in Fluid Mechanics (Academic Press, 1964).

Ladson, C. L., "Effects of independent variation of Mach and Reynolds numbers on the low-speed aerodynamic characteristics of the NACA 0012 airfoil section," NASA Technical Memorandum No. 4074, 1988.

McCroskey, W. J., "A critical assessment of wind tunnel results for the NACA 0012 airfoil," NASA Technical Memorandum No. 100019, 1987.

She, Z. S., Y. Wu, X. Chen, and F. Hussain, " A multi-state description of roughness effects in turbulent pipe flow," *New J. Phys.* 14, 093054(2012).

Perry, A. E., S. Hafez, and M. S. Chong, "Pitot probe corrections in fully devel- oped turbulent pipe flow," J. Fluid Mech. 439, 395–401 (2001).

Allen, J., M. Shockling, G. Kunkel, and A. Smits, "Turbulent flow in smooth and rough pipes," Philos. Trans. R. Soc. A 365, 699–714 (2007).

Clauser, F. H., "The turbulent boundary layer," Adv. Appl. Mech. 4, 1–51 (1956).

Colebrook, C. F., "Turbulent flow in pipes with particular reference to the transition region between the smooth and rough pipe laws," J. Inst. Civ. Eng. 11, 133–156 (1939).